Synthesis of arbitrary, two-mode, high-visibility N-photon interference patterns

Saroosh Shabbir, Marcin Swillo, and Gunnar Björk*

Department of Applied Physics, Royal Institute of Technology (KTH) AlbaNova University Center, SE-106 91 Stockholm, Sweden

(Received 7 February 2013; published 15 May 2013)

Using coherent states, linear optics, and N-photon detection we demonstrate the synthesis of arbitrary interference patterns and establish that neither the shape nor the visibility of N-photon interference patterns can be used as a quantum signature in general. Specific examples include saw-curve and rectangle-curve interference patterns and phase super-resolution with period shortening of up to 60 times compared to ordinary interference. The former two have visibility close to 100% and the latter has visibility in excess of 57%.

DOI: 10.1103/PhysRevA.87.053821 PACS number(s): 42.50.Ar, 42.25.Hz, 42.50.Dv

I. INTRODUCTION

The rapid development of experimental techniques has led to the demonstration of many remarkable quantum interference effects. A decade ago, it was shown that with specific N-photon quantum states, one could break the Rayleigh diffraction limit and make optical interference patterns with a smallest feature size N times smaller than with ordinary light [1]. This discovery laid the foundation for quantum lithography, and as the name conveys, it was thought that this was manifestly a quantum feature. However, superpositions and interference also manifest themselves in the classical world. It is therefore of interest to delineate what interference effects belong to the realm of the classical world and which require quantum states.

In different contexts limits arise for how large a visibility one can obtain using classical and quantum light. For instance, in the two-photon Hong-Ou-Mandel experiment, in principle one can achieve 100% visibility with both the input state $|1\rangle \otimes |1\rangle$ and the state $|1\rangle \otimes |\alpha\rangle$, where $|\alpha\rangle$ is a weak coherent state. However, two mutually phase randomized classical input states will never reach a visibility in excess of 50% [2]. Likewise, letting two classical states interfere in a Mach-Zehnder interferometer and measuring the probability of detecting m and $N-m$ photons respectively in the two output ports will never result in a visibility of the λ/N-period fringes $>50\%$ [3]. For three- and four-photon visibility experiments other limits to the obtainable visibility are 81.8% and 94.4%, respectively [4,5]. However, all these limits are derived with reference to a specific setup and a specific detection method. Here, we consider the interference between two coherent states using a general N-photon projection measurement (realized with linear optics and coincidence detection). In this case we show that there is no difference between classical and quantum states neither regarding the visibility (that can be 100% in both cases) nor in the obtainable shape of the interference curve. Only by restricting the measurements to $|m,N-m\rangle\langle m,N-m|$ projectors will one regain the results in Ref. [3]. The distinguishing quantum feature is instead the success probability. Only with quantum states can one surpass limits to, e.g., phase sensitivity of classical light [6,7]. This is regardless of the detection method.

*gbjork@kth.se

II. METHOD

A general, two-mode, N-photon state can be written

$$|\psi\rangle = \sum_{n=0}^{N} c_n |n,N-n\rangle = \sum_{n=0}^{N} b_n (\hat{a}^\dagger)^n (\hat{b}^\dagger)^{N-n} |0,0\rangle, \quad (1)$$

where $b_n = c_n/\sqrt{n!(N-n)!}$. If we formally divide $\sum b_n (\hat{a}^\dagger)^n (\hat{b}^\dagger)^{N-n}$ with $(\hat{b}^\dagger)^N$ and make the substitution $(\hat{a}^\dagger/\hat{b}^\dagger)^n = z^n$ we get the complex polynomial

$$\sum_{n=0}^{N} b_n z^n = b_N (z-z_1)(z-z_2)\cdots(z-z_N), \quad (2)$$

where we have used the fact that any complex Nth degree polynomial has exactly N complex roots. Hence, it is always possible to express any two-mode, N-photon state

$$|\psi\rangle = \frac{b_N}{\Pi_{n=1}^{N}\mathcal{N}_n} \mathcal{N}_1(\hat{a}^\dagger - z_1\hat{b}^\dagger)\cdots\mathcal{N}_N(\hat{a}^\dagger - z_N\hat{b}^\dagger)|0,0\rangle, \quad (3)$$

where $\mathcal{N}_n$ are real numbers such that $\mathcal{N}_n^2(1+|z_n|^2)=1$. Thus, any two-mode, N-photon state can be written as a direct product of N two-mode, single-photon states. Hofmann [8] made the important observation that to make a probabilistic projection measurement onto $|\psi\rangle\langle\psi|$, one could split the state to be measured into N two-mode paths and, using linear optics, unitarily transform the state in path n as $\mathcal{N}_n(\hat{a}^\dagger - z_n\hat{b}^\dagger)|0,0\rangle \to \hat{a}_n^\dagger|0,0\rangle$. Then, in the case where one detects one photon in the a_n mode of each path, one has in fact projected the input state onto $|\psi\rangle\langle\psi|$. It is convenient to use polarization states and, e.g., take the two modes a_n and b_n to be horizontally and vertically polarized modes. Then any single-photon polarization transformation can be achieved with two wave plates: The first compensates the relative phase between the a_n and b_n mode by $\theta_n = -\mathrm{Arg}(z_n)$ so that the (in general elliptically polarized) state $\mathcal{N}_n(\hat{a}_n^\dagger - z_n\hat{b}_n^\dagger)|0,0\rangle$ is transformed to the linearly polarized state $\mathcal{N}_n(\hat{a}_n^\dagger - |z_n|\hat{b}_n^\dagger)|0,0\rangle$, and the second is a polarizer rotated to the angle $\varrho_n = \arctan|z_n|$ so that the linearly polarized state passes it but the orthogonal polarization is blocked.

This method was further developed in Ref. [9] for measurement projection of NOON states, and demonstrated in [10,11] to project out the NOON state components from coherent states to demonstrate λ/N-period interference. In Ref. [12] the method was shown to provide a means of breaking the Heisenberg limit in interferometry when used

with a $|N/2,N/2\rangle$ state input. A similar method was used in Refs. [13,14] to demonstrate resolution beyond the Rayleigh limit using independent light sources, such as thermal light. A scheme to synthesize arbitrary filter functions from N cascaded polarization "components," based on a similar factorization was suggested [15] in 1967. However, in this proposal the individual components were frequency modes and not single-photon states.

The stated factorization method can be taken further. Suppose the input state is a two-mode, linearly polarized coherent state

$$|\alpha,\alpha\rangle = \exp(-|\alpha|^2)\sum_{m=0}^{\infty}\sum_{n=0}^{\infty}\frac{\alpha^{m+n}}{\sqrt{m!n!}}|m,n\rangle, \tag{4}$$

where for simplicity we take α to be real. We want to detect the interference between the phase-shifted input state and the projector $|\psi\rangle\langle\psi|$ where $|\psi\rangle$ is given by Eq. (1). The unitary, differential phase-shift operator is $\hat{U}(\phi) = \exp[-i\phi(\hat{a}^\dagger\hat{a} - \hat{b}^\dagger\hat{b})/2]$. The detected N-photon coincidence probability then becomes

$$\begin{aligned} P(\phi) &\propto |\langle\alpha,\alpha|\hat{U}^\dagger(\phi)|\psi\rangle|^2 \\ &= \alpha^{2N}\exp(-2\alpha^2)\left|\sum_{n=0}^{N} b_n \exp(i\phi[2n-N]/2)\right|^2 \\ &= \alpha^{2N}\exp(-2\alpha^2)\left|\sum_{n=0}^{N} b_n \exp(i\phi n)\right|^2. \end{aligned} \tag{5}$$

The sum within the absolute sign can be identified as a truncated Fourier series. Therefore, up to the highest "frequency" $N\phi/2$ in the parameter ϕ, any function can be expanded in the exponential function basis. This means that one can synthesize any interference curve with coherent-state input. That is, the N projector coincidence probability curve of N weak coherent states can be made exactly proportional to the N-photon coincidence probability curve of any quantum state.

However, splitting a polarization, two-mode coherent state $\hat{U}(\phi)|\alpha,\alpha\rangle$ spatially into N paths results in a product state of N identical coherent states $\hat{U}(\phi)|\alpha/\sqrt{N},\alpha/\sqrt{N}\rangle$. The fact that this is a product state makes each state's projection probability onto a certain single-photon projector, *viz.,*

$$P_n(\phi) = |\langle\alpha/\sqrt{N},\alpha/\sqrt{N}|\hat{U}^\dagger(\phi)\mathcal{N}_n(\hat{a}^\dagger - z_n\hat{b}^\dagger)|0,0\rangle|^2, \tag{6}$$

statistically independent of any other coherent state's projection probability [16]. The total probability is simply the product $P(\phi) = \Pi_{n=0}^{N} P_n(\phi)$ of the N individual projection probabilities. Thus, if one uses coherent input states it is not necessary to measure the "clicks" in each path in coincidence. Instead, each single-photon projector n can be measured separately using a weak coherent state. The result $P_n(\phi)$ is recorded, and the final probability $P(\phi)$ is subsequently obtained by multiplying all the individual probabilities as demonstrated for a NOON state in Ref. [11]. Hence, we need to implement only one of the arms in Fig. 1 at a time and reconfigure the bifrefringence θ_n and polarizer angle ϱ_n between each run. Note that this is only possible for coherent states. If, e.g., quantum states or thermal states are used, as is the case in Refs. [12] and [14], respectively, there are correlations between the different single-photon projection probabilities and a coincidence measurement is a must, whereas for coherent states either method works.

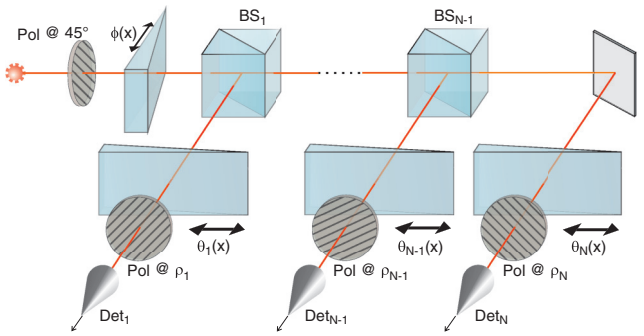

FIG. 1. (Color online) Projection measurement setup. A weakly excited two-mode coherent state, linearly polarized at 45 deg from the vertical, impinges from the left a birefringent wedge imparting the differential phase shift ϕ. It is subsequently divided by a sequence of nonpolarizing beam splitters into N paths. In each path, a certain single-photon state is projected out by preceding the detector with a polarizer set at ϱ_n and a birefringent wedge set to the differential phase θ_n. Finally the detection coincidences are recorded.

III. RESULTS

We have used a linearly polarized HeNe laser (whose polarization was further "cleaned" with a polarizer) with a power of 15 mW, neutral density filters, two birefringent wedges mounted on step-motor drive translators (with a precision of 1 μm), a polarizer mounted on a rotation stage (with a precision of 0.2 deg), and a single-photon sensitivity avalanche photo diode (APD). The intensity of the laser was adjusted by the neutral filters such that the mean time interval between two photons was 20 times longer ($\approx$1 μs) than the dead time of the detector (45 ns). Thus, we ensure that essentially each recorded "click" stems from a single photon. The laser's polarization was carefully adjusted to be 45 deg from the horizontal, thus creating the desired input state $|\alpha,\alpha\rangle$, where $\alpha \ll 1$ in the temporal mode basis of the detector. The calibration of the wedges was found to give a 2π phase shift with a relative translation of 0.215 mm.

To demonstrate the generality of the method, we first synthesized a rectangular interference pattern. That is, we would like to have

$$|\langle\alpha,\alpha|\hat{U}(\phi)|\psi_s\rangle|^2 \propto f_{Rect}(\phi,\pi/2) = \begin{cases} 0 & |\phi| \leqslant \pi/2, \\ 1 & \text{otherwise.} \end{cases} \tag{7}$$

To this end, for $N = 30$ which gives a reasonable rectangle-like function, we compute the 31 lowest Fourier expansion coefficients of f_{Rect} and identify the coefficients with the expansion coefficients b_n in Eq. (5). Subsequently the expansion is factored in single-photon projector terms by Eqs. (2) and (3) (see the Appendix). The 30 single-photon projectors are then measured and multiplied. The result is displayed in Fig. 2 where the only fitting is the amplitude of the theoretically predicted coincidence probability. The experimental curve represents raw data; no background subtraction or any other data processing have been done. The maximum count rate

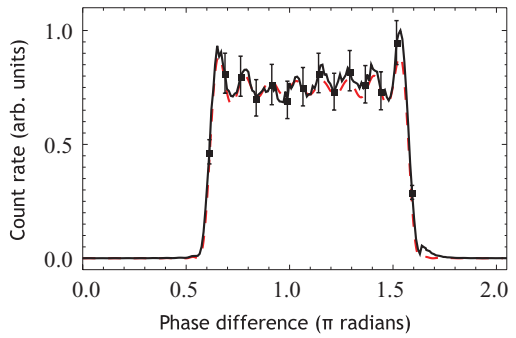

FIG. 2. (Color online) Rectangular interference pattern. The solid (black) line (215 data points) shows raw data and the dashed (red [gray]) line shows the theoretically expected curve with the amplitude chosen for best fit. At selected data points, error bars show the $\pm\sigma$ statistical uncertainty.

employed in the experiments was around 5.2 MHz. A discussion about the error bars will follow below.

Next, we synthesized a Saw-curve interference pattern. The interference pattern is the square of the overlap between the input state and the projector, and we want the (2π-periodic) overlap between the input state and the measurement projector to be

$$|\langle\alpha,\alpha|\hat{U}(\phi)|\psi\rangle| = |\phi/\pi|^{1/2} \tag{8}$$

in the interval $\{-\pi,\pi\}$. Again by finding the Fourier coefficients for $N = 30$, plugging them into Eq. (2), and factorizing the polynomial to obtain the single-photon projectors (see the Appendix), we finally get the raw data displayed in Fig. 3 where the only fitting is the amplitude of the theoretically predicted curve. This interference pattern has the particular feature that its derivative, which governs the phase sensitivity, is almost constant over large intervals.

Finally, a NOON state

$$|\psi_{\mathrm{NOON}}\rangle = \frac{1}{\sqrt{2}}\left(|N,0\rangle - |0,N\rangle\right), \tag{9}$$

can give an interference pattern with the smallest feature size $\approx\lambda/(2N)$, where λ is the wavelength of the light [1]. This feature size reduction can be explained in terms of maximizing a state's dynamical evolution speed [17–20] or in terms of N-photon quasiparticles having N times the linear momentum

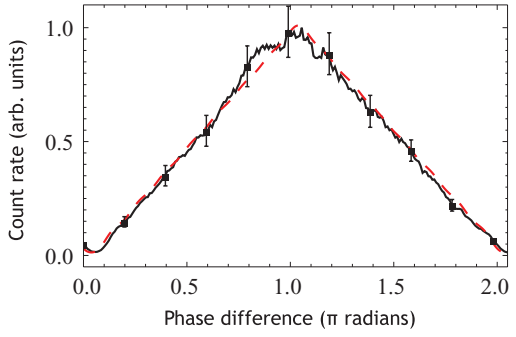

FIG. 3. (Color online) Saw-curve interference pattern. The solid (black) line shows raw data and the dashed (red [gray]) line shows the theoretically expected curve with the amplitude chosen for best fit. At selected data points, error bars show $\pm\sigma$ statistical uncertainty.

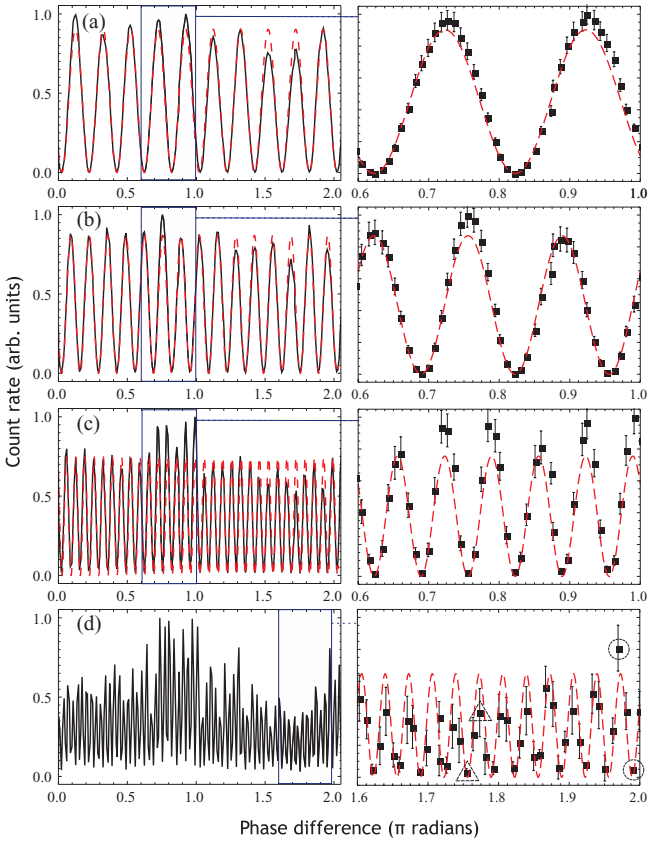

FIG. 4. (Color online) NOON-state coincidence patterns. In the figures on the left, the solid (black) lines represent raw data points connected by straight lines. No background subtraction has been done. The dashed (red [gray]) curves are the expected $A\sin^2(N\phi/2)$ with A chosen for best fit. The figures on the right show a magnified part of the data points with error bars and the fit curve. Error bars show $\pm\sigma$ statistical uncertainty. (a) $N = 10$. (b) $N = 15$. (c) $N = 30$. (d) $N = 60$. The boxed area shows the portion with highest visibility, with the maximum of 88.1% occurring at 1.98π. The circles show the points used for calculating maximum visibility. The triangles show the points with a more probable high visibility of 86.2% at 1.75π.

of the photons making up the quasiparticles and thus having a de Broglie wavelength N times smaller [21–24]. Up to now, there have been many proposals and demonstrations [2,9–11,22–28] of NOON-state interference with $N = 2$ to $N = 30$. The $N = 6$ to $N = 30$ experiments [10,11] were made with coherent light with the same method we now generalize. There has also been other demonstrations and proposals of multiphoton (i.e., using coincidence measurements) interference using nonentangled, classical states also showing a period shortening, but at the expense of a reduced interference visibility. In, e.g., Ref. [3] periods down to 1/4 of the "regular" interference period were measured, but with a visibility of only about 29%. Using the method above, we obtained interference patterns for projection of a coherent state onto $N = 10$, 15, 30, and 60 NOON state projectors, shown in Fig. 4. We see that for $N = 10$ we get an excellent fit with the predicted pattern. The poorest visibility, where the visibility of a fringe is defined by the adjacent local minimum and local maximum of the interference pattern, is 99.5% in this case. Even for

$N = 60$ we get a reasonable fit with the theory and minimum and maximum visibilities of 57.5% and 86.2%.

The visibility is limited by five effects. The first one is the smallest step with which we can vary ϕ. It is set by the combination of birefringent material (quartz in our case), the birefringent wedge angle which is 19 deg, and the linear motorized stage minimum step size 1 μm. This leads to a minimum phase difference resolution of 29 mrad, which for $N = 60$ is too poor (one period of the pattern, occupying $2\pi/60$ rad, is probed by less than four measurement points). As seen in Fig. 4(d), we simply "miss" many minima and maxima of the pattern, yielding a lower visibility than that set by other measurement errors and noise. For $N \leqslant 30$, the dominant source of error is the stochastically varying quantum efficiency of the detector. The measured coincidence probability is $P(\phi) = \Pi_{n=1}^{N} \eta_n P_n(\phi)$, where η_n is the quantum detector efficiency for the single-photon projector n. In our case, we use the same detector for each projector, and therefore $\eta_n \to \eta(n\tau)$, where $\tau = 480$ s is the time it took between measuring the point ϕ of one projector to the same point for the next projector. Assuming that the variation in quantum efficiency $\Delta\eta(n\tau) = \eta(n\tau) - \langle\eta(\tau)\rangle$ is uncorrelated between one projector and another, the expected standard deviation due to this error is

$$\langle[\Delta P(\phi)]^2\rangle^{1/2} = \sqrt{N} P(\phi) \frac{\langle[\Delta\eta(n\tau)]^2\rangle^{1/2}}{\eta}. \qquad (10)$$

This equation shows two important features. First, due to the multiplication of detection events the error will grow with the square root of the projector's photon number. This sets an upper limit to the method's applicability. Second, the absolute error is proportional to the coincidence probability; stated otherwise, the relative error is constant. This is clearly seen in our data as an excellent fit between experiment and theory as long as $P(\phi)$ is small. Another error source, but less important for our measurements, is small errors in the phases θ_n. For a rapidly oscillating function, the exact position of each single-photon projector's minimum has a substantial impact, as predicted in Ref. [29]. In addition, for the NOON state interference, one should ideally be able to get all the light in and out of one linear polarizer. At best, we manage a perpendicular polarization suppression ratio of 46 dB, and typically the suppression rate is >40 dB. Finally, the detector dark count also sets a limit. For our NOON-state interference this error source is negligible as the dark count rate is <2 Hz and the maximum count rate is 1.02 MHz. The detector efficiency (if it were constant) does not matter in the experiment as the detected state is a coherent state irrespective of n and ϕ. A low detector efficiency (about 20% for our detector) can easily be offset by a higher input intensity.

IV. CONCLUSIONS

With the Hofmann-Guo method [8,9], it is possible to synthesize any interference pattern to, in principle, the precision given by N. The method does not limit the obtainable visibility, and we have shown that in practice, even $N = 60$ NOON-state interference patterns can be recorded with >50% visibility. We have also demonstrated that unusual (nonsinusoidal) interference patterns can arise from multiphoton interference of coherent states. Hence, it is neither the shape nor the visibility of multiphoton interference patterns that delineate a general border between classical and quantum interference, although in special cases limits do apply.

However, with a coherent state input it is not possible to get quantum phase sensitivity [6,7,26] (i.e., break the standard quantum limit [30,31]). On the contrary, as discussed in some detail in Ref. [11], for a given mean photon number, e.g., the NOON state, interference curves have a lower phase sensitivity than ordinary (single-fringe) interferometry with a coherent state.

It is possible to directly scale up the demonstrated method to the classical regime using ordinary photo detectors, and perhaps it is here the method will find applications. In this case the single-photon detector can be replaced by, e.g., an ordinary Si photodiode and the photon number could be increased to the classical regime, i.e., millions or billions of photon per mode. Both Eqs. (5) and (10) would still be valid with $P(\phi)$ now being proportional to the photocurrent. The limit on N imposed by Eq. (10) still holds. It simply does not matter if it is a classical or a quantum detector's efficiency that fluctuates. Despite this, one reason we have stuck to working at the single-photon detection level is to show that the coincidence method is very flexible in that it allows the synthesis of *any* two-mode, multiphoton projector, albeit at the expense of exponentially decreasing probability of coincidence events with increasing N. Another reason is to explore what practical limits (i.e., the influence of various sources of errors) one encounters when one scales single-photon coincidence measurements to large numbers.

When using coherent-state input, the switch from obtaining the interference curves by coincidence measurements to multiplication of single-photon projection probabilities allows considerable savings in time and equipment. In our case, the maximum probability of detecting a photon in a single temporal mode, defined by the response time of the detector, is about 0.1 for each single-photon projector. Hence, as the N single-photon projectors give statistically independent results, the probability of detecting, say, 10 photons in coincidence would be around $0.1^{10} = 10^{-10}$. With our detectors with a response time of 45 ns it would thus take at least $45 \times 10^{-9} \times 10^{10} = 450$ s to get a single coincidence click, on average. When detecting each (temporal) mode sequentially, instead of detecting N (spatial) modes in parallel, it took about 900 s to measure the 60 projectors for a single phase shift ϕ. Thus, by taking 215 steps to cover the range of phase shifts from 0 to 2π rad, a whole $N = 60$ interference curve was obtained in about 8 h, which is long but feasible.

ACKNOWLEDGMENTS

The authors thank C. Kothe, S. Takeuchi, K. Edamatsu, and S. Harris for helpful discussions. The work was supported by the Swedish Research Council (VR) through Grant No. 621-2011-4575 and by the Linnæus Excellence Center ADOPT.

APPENDIX: FOURIER EXPANSION COEFFICIENTS

Consider a 2π-periodic rectangle function defined by the two conditions

$$f_{Rect}(\phi,\pi/2) = \begin{cases} 0 & |\phi| \leqslant \pi/2, \\ 1 & \text{otherwise.} \end{cases} \qquad (A1)$$

and $f_{Rect}(\phi,\pi/2) = f_{Rect}(\phi + 2l\pi,\pi/2)$, where l is an arbitrary integer. Since f_{Rect} is even, it is advantageous (and natural) to use an even number of projectors to synthesize the function, implying that N should be chosen even. (The function can also be expanded for odd N but with a less pleasing result.) The Fourier expansion of this function can hence formally be written

$$f_{Rect}(\phi,\pi/2) = \sum_{n=-N/2}^{N/2} b_{(2n+N)/2} \exp(i\phi n), \tag{A2}$$

where the expansion coefficients are

$$b_{(2n+N)/2} = \frac{1}{2\pi}\int_{-\pi}^{\pi} f_{Rect}(\phi,\pi/2)\exp(-i\phi n)d\phi \tag{A3}$$

$$= \begin{cases} 1/2 & n = 0, \\ -\frac{\sin(n\pi/2)}{n\pi} & n \neq 0, \end{cases} \tag{A4}$$

By using Eq. (1), the associated polynomial for this state for, e.g., $N = 10$, is hence

$$\frac{z^5}{2} - \frac{z^4 + z^6}{\pi} + \frac{z^2 + z^8}{3\pi} - \frac{1 + z^{10}}{5\pi} = 0, \tag{A5}$$

with the roots

$$\begin{aligned} z_1 = z_2^* &= 0.967612 + i0.252442, \\ z_3 = z_4^* &= 0.723141 + i0.6907, \\ z_5 = z_6^* &= 0.313207 + i0.949685, \\ z_7 = z_8^* &= -0.463687 + i0.29332, \\ z_9 = z_{10}^* &= -1.54027 + i0.974347. \end{aligned} \tag{A6}$$

The fact that f_{Rect} is an even function leads to the result that all the roots of the associated polynomial come in complex conjugate pairs. By inserting these roots into Eq. (3) it is evident how to implement the 10 single projectors. For example, the $n = 1$ projector is implemented by introducing a birefringence of $-\mathrm{Arg}(z_1) \approx -0.255$ rad $= -14.6$ deg between the horizontal and vertical directions. This birefringence should be followed by a polarizer set at the angle $\arctan|z_1| = \pi/4$ rad. In Table I we list the settings of the birefringence and the polarizer angle for the 10 projectors in degrees.

It is seen in Fig. 2 that the resulting function is not a perfect rectangle, but the Gibbs phenomenon makes the interference curve overshoot on the steep flanks. This effect can be reduced by the use of a Lanczos-Fourier expansion or a Cesàro approximation of the Fourier series, at the expense of getting less steep flanks in both cases. By going to higher photon numbers one could in principle reduce the wiggles in the interval $\{\pi/2,3\pi/2\}$, but the overshoot height would remain the same; only the width of the overshooting peak could be decreased.

In a similar manner, an $N = 10$ expansion of ${f_{Saw}}^{1/2}$ is

$$f_{Saw}^{1/2}(\phi,2\pi) = \sum_{n=-N/2}^{N/2} b_{(2n+N)/2}\exp[-i\phi n]. \tag{A7}$$

By computing the expansion coefficients in the same manner as before, one arrives at

$$b_{(2n+N)/2} = \frac{\sqrt{2n}\sin(n\pi) - f_{FS}(\sqrt{2n})}{\sqrt{2}\pi n^{3/2}}, \tag{A8}$$

where f_{FS} is the Fresnel sine function. Numerically, the coefficients are

$$\begin{aligned} b_5 = 2/3, \quad b_4 = b_6 = -0.1607, \\ b_3 = b_7 = -0.0273, \quad b_2 = b_8 = -0.0272, \\ b_1 = b_9 = -0.0109, \quad b_0 = b_{10} = -0.0121. \end{aligned} \tag{A9}$$

The polynomial associated to the expansion is thus

$$\begin{aligned} \frac{2z^5}{3} - 0.1607(z^4 + z^6) - 0.0273(z^3 + z^7) - 0.0272(z^2 + z^8) \\ - 0.011(z + z^9) - 0.012(1 + z^{10}) = 0 \end{aligned} \tag{A10}$$

with the roots

$$\begin{aligned} z_1 = 1.49215, \quad z_2 = 0.670175, \\ z_3 = y_4^* = 0.637336 + i2.22359, \\ z_5 = y_6^* = 0.119116 + i0.415582, \\ z_7 = y_8^* = -0.311654 + i0.245907, \\ z_9 = y_{10}^* = -1.97752 + i1.56034. \end{aligned} \tag{A11}$$

The settings, in degrees, for the birefringence and the polarizer angle are given in Table II.

TABLE I. The experimental parameters for $N = 10$ f_{Rect} projectors.

Root n	ϱ_n	θ_n
1	45.0	− 14.6
2	45.0	14.6
3	45.0	− 43.7
4	45.0	43.7
5	45.0	− 71.7
6	45.0	71.7
7	28.7	− 147.7
8	28.7	147.7
9	61.2	− 147.7
10	61.2	147.7

TABLE II. The experimental parameters for $N = 10$ f_{Saw} projectors.

Root n	ϱ_n	θ_n
1	56.2	0.0
2	33.8	0.0
3	66.6	− 74.0
4	66.6	74.0
5	23.4	− 74.0
6	23.4	74.0
7	21.7	− 141.7
8	21.7	141.7
9	68.3	− 141.7
10	68.3	141.7

[1] A. N. Boto, P. Kok, D. S. Abrams, S. L. Braunstein, C. P. Williams, and J. P. Dowling, Phys. Rev. Lett. **85**, 2733 (2000).
[2] J. G. Rarity, P. R. Tapster, E. Jakeman, T. Larchuk, R. A. Campos, M. C. Teich, and B. E. A. Saleh, Phys. Rev. Lett. **65**, 1348 (1990); J. G. Rarity, P. R. Tapster, and R. Loudon, J. Opt. B: Quantum Semiclass. Opt. **7**, S171 (2005).
[3] I. Afek, O. Ambar, and Y. Silberberg, Phys. Rev. Lett. **104**, 123602 (2010).
[4] Z. Ficek and S. Swain, *Quantum Interference and Coherence: Theory and Experiments* (Springer, New York, 2005).
[5] I. N. Agafonov, T. Sh. Iskhakov, A. N. Penin, and M. V. Chekhova, JETP Lett. **85**, 381 (2007).
[6] T. Nagata, R. Okamoto, J. O'Brien, K. Sasaki, and S. Takeuchi, Science **316**, 726 (2007).
[7] R. Okamoto *et al.*, New J. Phys. **10**, 073033 (2008).
[8] H. F. Hofmann, Phys. Rev. A **70**, 023812 (2004).
[9] F. W. Sun, Z. Y. Ou, and G. C. Guo, Phys. Rev. A **73**, 023808 (2006).
[10] K. J. Resch, K. L. Pregnell, R. Prevedel, A. Gilchrist, G. J. Pryde, J. L. O'Brien, and A. G. White, Phys. Rev. Lett. **98**, 223601 (2007).
[11] C. Kothe, G. Björk, and M. Bourennane, Phys. Rev. A **81**, 063836 (2010).
[12] F. W. Sun, B. H. Liu, Y. X. Gong, Y. F. Huang, Z. Y. Ou, and G. C. Guo, Europhys. Lett. **82**, 24001 (2008).
[13] R. Wiegner, C. Thiel, J. von Zanthier, and G. S. Agarwal, Opt. Lett. **36**, 1512 (2011).
[14] S. Oppel, T. Büttner, P. Kok, and J. von Zanthier, Phys. Rev. Lett. **109**, 233603 (2012).
[15] S. E. Harris, E. O. Ammann, and I. C. Chang, J. Opt. Soc. Am. **54**, 1267 (1964).
[16] R. J. Glauber, Phys. Rev. **130**, 2529 (1963); **131**, 2766 (1963).
[17] N. Margolus and L. B. Levitin, Phys. D (Amsterdam, Neth.) **120**, 188 (1988).
[18] B. C. Sanders, Phys. Rev. A **40**, 2417 (1989).
[19] J. Söderholm, G. Björk, T. Tsegaye, and A. Trifonov, Phys. Rev. A **59**, 1788 (1999).
[20] H. Lee, P. Kok, and J. P. Dowling, Mod. Opt. **49**, 2325 (2002).
[21] J. M. Jacobson, G. Björk, I. Chuang, and Y. Yamamoto, Phys. Rev. Lett. **74**, 4835 (1995).
[22] E. J. S. Fonseca, C. H. Monken, and S. Padua, Phys. Rev. Lett. **82**, 2868 (1999).
[23] K. Edamatsu, R. Shimizu, and T. Itoh, Phys. Rev. Lett. **89**, 213601 (2002).
[24] P. Walther *et al.*, Nature (London) **429**, 158 (2004).
[25] M. D'Angelo, M. V. Chekhova, and Y. H. Shih, Phys. Rev. Lett. **87**, 013602 (2001).
[26] M. W. Mitchell, J. S. Lundeen, and A. M. Steinberg, Nature (London) **429**, 161 (2004).
[27] I. Afek, O. Ambar, and Y. Silberberg, Science **328**, 879 (2010).
[28] Y. Israel, I. Afek, S. Rosen, O. Ambar, and Y. Silberberg, Phys. Rev. A **85**, 022115 (2012).
[29] P. Kok, Opt. Spectrosc. (USSR) **111**, 520 (2011).
[30] C. M. Caves, Phys. Rev. Lett. **45**, 75 (1980).
[31] V. Giovannetti, S. Lloyd, and L. Maccone, Science **306**, 1330 (2004).